Localized Measurement of a Sub-Nanosecond Shockwave Pressure Rise Time

Jaka Petelin, Žiga Lokar, Darja Horvat, and Rok Petkovšek

***Abstract*— In a growing number of applications, fast and localized pressure measurement in aqueous media is desired. To perform such measurements, a custom-made single-mode fiber-optic probe hydrophone (FOPH) was designed and used to measure the pressure pulse generated by laser-induced breakdown (LIB) in water. The sensor enabled sub-nanosecond pressure rise time measurement. Both the rise time and the duration of the shockwave were found to be shorter in the direction perpendicular to the breakdown generating laser beam, compared to the shockwave observed in the parallel direction. Simultaneous high-frame-rate imaging was used to qualitatively validate the novel hydrophone data and to observe the shockwave evolution. The measurements were performed also on pressure pulses emitted during the generation of miniature (150 μm diameter) laser-induced bubbles at very small distances (down to 40 μm), further demonstrating the capabilities of the small-size sensor and the ability to measure locally. The results improve understanding of LIB shockwave characteristics dependence on laser pulse energy and duration.**

***Index Terms*— Fiber-optic probe hydrophone (FOPH), pressure, shockwave.**

I. Introduction

VERY-SHORT and high-pressure transients in fluids, both compressive and tensile, are produced in a growing number of industrial and medical applications, for example in laser-induced breakdown (LIB) spectroscopy [1], shock cleaning [2], sonoporation [3], high intensity focused ultrasound removal of tumors [4], shock wave lithotripsy [5], [6], and laser vitreolysis [7]. Along with this development, the need to measure and monitor these short events is also increasing in importance [6].

Energy input accompanying pulsed laser medical procedures often results in the generation of shockwaves with locally extremely high positive and negative pressures of several tens of MPa which cause unwanted damage to the tissue. To minimize the impact on the surrounding tissue the current trends are going in the direction of using smaller laser pulse energies and shorter pulses. It is important to accurately measure the pressure values as close to the source as possible, spatially, and temporally, since this enables direct evaluation of peak pressures as they are encountered for example by living cells during laser medical procedures like vitreolysis, sonoporation, or lithotripsy, without having to rely on estimates of linear decay of shockwave pressure with distance [8]. The present contribution is a step in this direction.

There are multiple approaches to measure these transient signals, like piezoelectric sensor [9], [10], polyvinylidene fluoride (PVDF) membrane [11]–[13] or needle hydrophone [14], [15], and fiber-optic hydrophone [16]–[18], all with their own advantages and drawbacks. In the case considered here, i.e., measurement of shockwave emitted during LIB in water, the fiber-optic probe hydrophone (FOPH) comes with a key advantage—the ability to measure and withstand very quick changes of very high positive or negative pressures that are generated during breakdown [19].

There are several types of fiber-optic hydrophones, many of them based on building an additional structure placed at the fiber tip. A lot of research is focused on improving sensor sensitivity to accurately detect low pressure [20]. A Fabry–Perot based interferometric design is very common [21]–[23], while other structures are considered, too [24]–[27]. The type of fiber hydrophone considered here is based on reflectance changes at the water–glass interface due to the pressure-induced changes of the refractive index of water. The design was introduced by Staudenraus and Eisenmenger [16] and is often referred to as Eisenmenger type hydrophone [28]. The sensing element is the interface itself between the aqueous medium and the end face of the optic fiber core. While this simpler approach offers less sensitivity, it allows for a quick repair of any damage to the sensing element by simply re-cleaving the damaged part of the fiber end [29]. Additionally, as the measurement of water pressure is direct, this approach has the potential to offer the fastest sensor response.

FOPH of Eisenmenger type is typically based on multimode fibers, although some single-mode hydrophones were fabricated [30]. Single-mode fibers are less sensitive than their multimode counterparts due to the lower laser light power and have stronger oscillations in frequency response, especially at lower (<100 MHz) frequencies [31]. However, their advantage is a significantly smaller sensor area with fiber core having only a few micrometers diameter compared to tens of micrometers for a typical multimode fiber. A more point-like detector, therefore, helps to accurately measure the pressure at a specific point [32] as well as offers higher sensor bandwidth in realistic configurations. Especially localized measurement is of interest for the study of sonoporation [33].

Manuscript received May 30, 2021; accepted September 21, 2021. Date of publication September 24, 2021; date of current version December 30, 2021. This work was supported by the Slovenian Research Agency (ARRS) funding program under Program P2-0270, Project L2-9254, and Project L2-9240. *(Corresponding author: Rok Petkovšek.)*

The authors are with the Faculty of Mechanical Engineering, University of Ljubljana, 1000 Ljubljana, Slovenia (e-mail: rok.petkovsek@fs.uni-lj.si).

Digital Object Identifier 10.1109/TUFFC.2021.3115629

First, we present single-mode FOPH measurements of shockwaves emitted by a dielectric breakdown generated in water by laser pulses having a few nanoseconds of duration and a few millijoules of energy. Sub-nanosecond pressure rise time is observed during light-induced breakdown. Significant differences are observed between the results of measurement with hydrophone oriented in the direction parallel and perpendicular to the generating laser pulse direction. Pressure measurement is accompanied by simultaneous imaging of the shockwave using our fast illumination system [34]. These measurements are followed by measurements of shockwave generated during a significantly lower energy (10 μJ) LIB in water at very small distances, down to 40 μm.

II. Principle of Operation

Reflectance FOPH is based on measuring the variation in reflectance at the glass–water interface due to pressure wave arriving at the sensor. The refractive index of water n changes with pressure p by [35]

$$\frac{\Delta n}{\Delta p} = 1.31 * 10^{-4}\ \text{MPa}^{-1}. \tag{1}$$

The value of the coefficient is temperature-dependent and valid for pressures up to approximately 100 MPa. The change of refractive index leads to a change in light reflectance at the fiber–water interface, measured by a photodiode that detects the intensity of the reflected light inside the fiber. The hydrophone voltage signal information, therefore, has two components–the steady-state signal (dc component) U_0 corresponding to the light reflectance at the glass–water interface at initial pressure (usually 1 bar), and voltage variations ΔU due to transient pressure changes. Using (1), the values of refractive index for water and quartz at standard conditions (1.32 and 1.45, respectively) and the Fresnel equations for reflectance, the pressure change is calculated to be

$$\frac{\Delta p}{\Delta U} = \frac{458}{U_0}\ \text{MPa}^{-1}. \tag{2}$$

The raw measured pressure data need to be deconvolved using the sensor frequency response function to obtain the actual pressure in the liquid. The deconvolution is performed by division of the Fourier transform of the raw measured pressure by calculated or preferably measured fiber sensor response, and then inverse Fourier transform is performed to obtain actual pressure profile in the time domain. To account for the acoustic reflection at the water–glass rigid interface, for the purpose of this study, a factor of 2 is assumed for convenience. The pressure dependence of the quartz glass refractive index can be neglected because of its low compressibility and because most of the shockwave is reflected.

In an effort to improve on the state of the art of measuring short rise time phenomena like the arrival of a shockwave pressure front [36], we used a single-mode fiber as the sensing element of the hydrophone. The small dimension of the single-mode fiber core (5 μm) is the key feature that results in: 1) a more localized measurement, 2) less sensitivity to positioning tilt, and 3) faster response time, as explained in more detail below. The details of local measurement of a fast phenomenon are illustrated in Fig. 1.

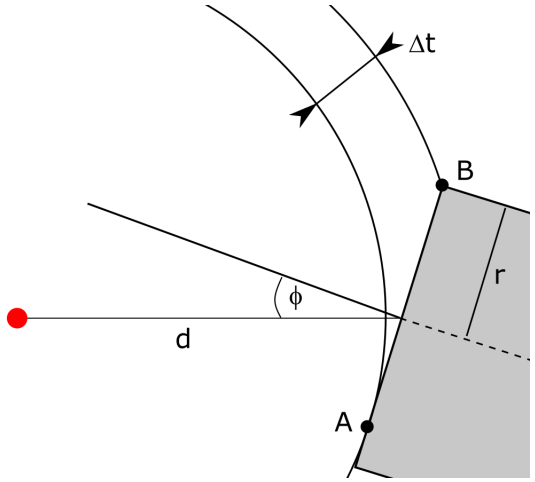

Fig. 1. Schematic of fiber positioning with respect to the laser-induced breakdown position and orientation (breakdown marked with a red dot). The fiber with a core of radius r (cladding is not shown) is positioned at a distance d from the breakdown and oriented so that the fiber geometrical axis is at an angle Φ with respect to the line connecting the center of the breakdown and the center of the fiber end face. The pressure transient emitted from the breakdown reaches different parts of the fiber end face at different times. The time interval between the shockwave front first reaching the fiber (at point A) and the last (at point B) is marked with Δt and is a function of r, d, and Φ as shown in (3).

An arbitrary fiber position and orientation with respect to the LIB can be described by two parameters: 1) the distance d between the LIB and the fiber end face center and 2) the angle Φ between the line d and the fiber geometry axis. The shockwave is emitted from the LIB (red dot on the left) and propagates uniformly in all directions. Because of the finite fiber lateral dimension, the different parts of the shockwave reach the fiber tip at different times. The sensor performs spatial convolution over the sensing area of the fiber end face, resulting in the temporal signal being a weighted average of contributions. The time interval between the pressure front reaching the first point on the fiber end face (point A) and the last one (point B) is marked with Δt. The last point is always at the core edge, while the first may be anywhere between the center and the other edge, depending on the fiber core radius and positioning. Effects of the reflection of the shockwave from the fiber end are neglected in this consideration.

This time interval Δt corresponds to the time over which the sensor averages the signal, resulting in temporal broadening of the sensor output. It should therefore be as small as possible to allow quick response and to accurately measure the sharp shockwave front.

Assuming constant pressure front velocity v, the time interval Δt can be calculated from the difference Δd between the path d_A that the wave travels to point A and path d_B to point B

$$\Delta d = \sqrt{d^2 + 2dr\sin(\phi) + r^2} - \begin{cases} d\cos(\phi), & \text{if } d\,\tan(\phi) < r \\ \sqrt{d^2 - 2dr\sin(\phi) + r^2}, & \text{otherwise.} \end{cases} \tag{3}$$

To obtain Δt, this expression is simply divided by the wave velocity v

$$\Delta t = \frac{\Delta d}{v}. \tag{4}$$

In the consideration, we assumed that $0° \leq \phi \leq 90°$ and the absolute value is required for negative angles. While point B is always the farthest point from the breakdown at the fiber edge, the nearest point A may be located either at the edge or somewhere on the fiber end face (for example at the fiber center for $\Phi = 0°$), resulting in a branched (3).

For simplicity, the wave velocity in water v is assumed constant at 1500 m/s–i.e., the acoustic velocity in water. In reality, the shock wavefront initially propagates with significantly higher (supersonic) velocity. Because of the rapid dissipation of energy, the velocity of the shockwave front in the water soon drops to the acoustic velocity. For laser excitation pulses in the millijoule range, this drop occurs in a few tens of a millimeter, whereas shockwaves arising from microjoule pulses slow down even sooner [8], [37]. Moreover, since the velocity is higher only for a short period of time after the breakdown, the correction is the same for both distances, d_A and d_B, and is canceled by their subtraction in (3). Therefore the qualitative findings explained below are still valid.

Using (4), Δt is calculated for the two common fiber core dimensions at various distances d and tilt angles Φ to illustrate the advantage of a single-mode fiber having a small fiber core with a diameter of 5 μm, compared to a multimode fiber with a fiber core diameter of 50 μm. The results of the calculation are presented in Fig. 2.

The advantage of a small sensing element is shown to be both in better time resolution resulting also in shorter response time as well as in tolerance to inaccurate tilt positioning. We consider how accurately a fiber sensor has to be positioned with respect to the fiber tilt angle Φ so as not to exceed a certain value of Δt. The value is chosen here to be 1 ns, the approximate shockwave pressure rise time in water in the case of nanosecond laser pulse excitation [8]. A multimode fiber needs to be positioned within 1.5° so as not to exceed the selected 1 ns threshold for large distances (>1 mm), whereas the single-mode fiber satisfies the same condition at a 15° positioning tilt angle (not shown in Fig. 2). Additionally, because of its relatively large lateral dimension, even perfect positioning of the multimode fiber (with no tilt) is not sufficient to meet the threshold for distances below 200 μm, whereas the smaller single-mode fiber in the no tilt case comfortably stays below the selected threshold even for a very small distance of 10 μm. Therefore, for sufficiently fast measurements at short distances, single-mode fiber is required.

This approximation is limited to the analysis of fiber response to infinitely sharp shockwaves emitted from a point source. Shockwave diffraction on fiber edges is not considered in this approximation, while plasma is assumed to consist of many independent point-like sources of shockwaves. Considering the dimensions of the single-mode fiber used in the experiments, this approximation is valid from the arrival of the shockwave for approximately 40 ns at 0° fiber tilt, when the diffracted reflected waves from the fiber cladding edge

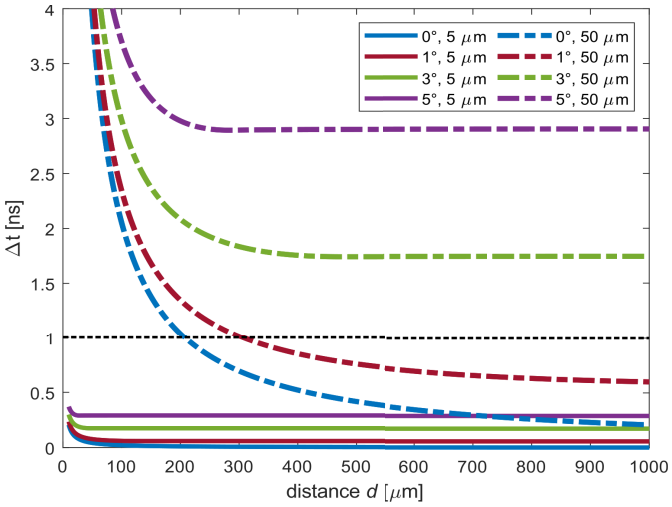

Fig. 2. Time interval Δt as a function of distance d for two different fiber core diameters 5 μm (single-mode) and 50 μm (multimode) and different fiber tilts Φ (0°, 1°, 3°, and 5°). The 1 ns threshold is shown as a dashed black line. Measurements below the threshold are sufficiently fast to accurately record the shockwave edge.

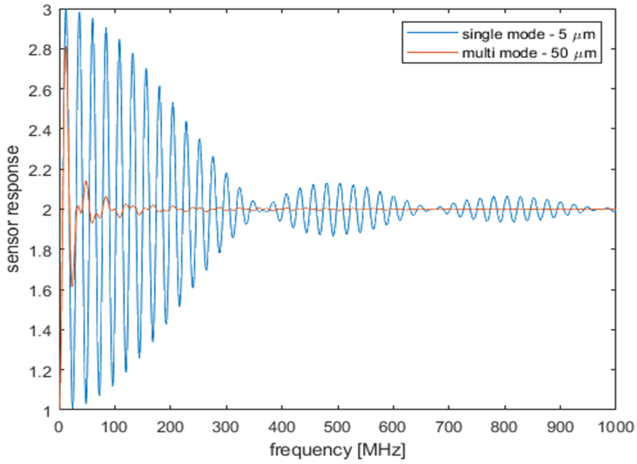

Fig. 3. Modeled frequency response function of the 5/125 μm single-mode fiber. The multimode fiber response is added for comparison.

(approximately 60 μm from the core) reach the fiber core. We additionally assume the fiber is perfectly rigid.

For signal duration beyond 40 ns (sooner with non-zero fiber tilt), these reflections need to be taken into account. We have performed the analysis of rigid fiber approximation with plane wave incident perpendicular to fiber (as in [31]), shown in Fig. 3.

The single-mode fiber frequency response shows significant oscillations for the first few hundred MHz, while the oscillations are significantly lower at higher frequencies, above 300 MHz, the frequency corresponding to approximately 1 ns rise time. The frequency response of a multimode fiber (50 μm core) is added for comparison. We believe that our single-mode fiber sensor is positioned in the optimum range for fast and accurate measurement on time scales close to the 1 ns—an even smaller fiber core would exhibit higher amplitude oscillations in the frequency response function at these time scales, while larger fiber cores have higher Δt (Fig. 2). The results

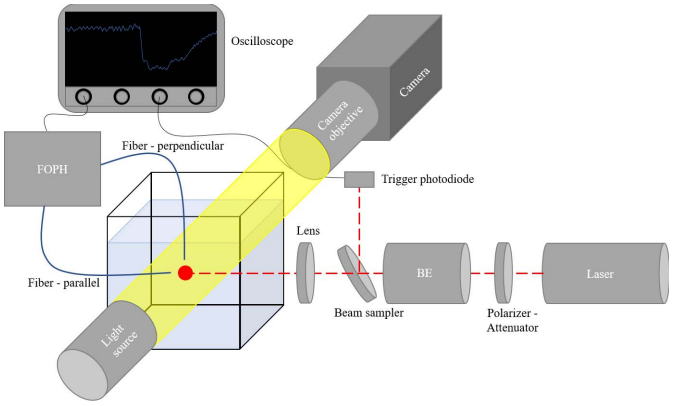

Fig. 4. Experimental setup. The laser pulse (10 μJ to 15 mJ) produces breakdown in water, recorded by a camera and the FOPH. The details of fiber positioning with respect to breakdown are shown in Fig. 1 for parallel orientation.

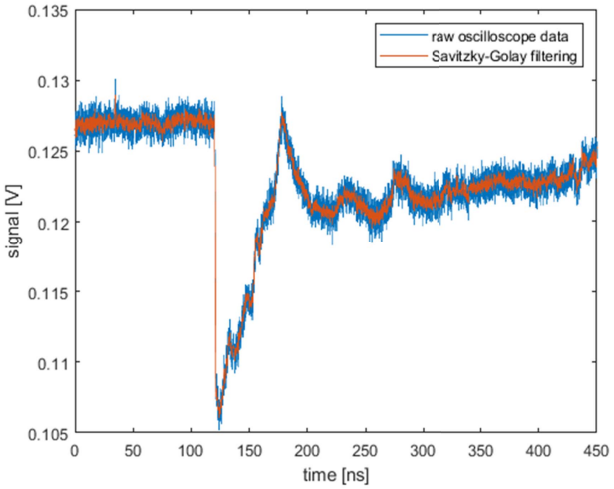

Fig. 5. Raw fiber-optic pressure sensor output voltage when measuring laser-induced shockwave. The average signal value up to 120 ns is constant (except for the 2 mV noise) and corresponds to the pressure of 1 bar. Signal filtered by Savitzky–Golay filter (order 2, frame length 250 ps) shows significantly improved signal-to-noise ratio while following the shockwave trends. The pressure front arrival at 120 ns is seen as a sharp signal fall followed by a slower and jagged recovery.

of the calculation are mainly of interest for lower frequency signals, the very sharp shockwave edge is not expected to be influenced. It needs to be pointed out that both analyses are simplified although under different sets of assumptions. However, calculating the exact sensor response function to the incident shockwave from a finite source including fiber deformation or its resonances is beyond the scope of this study.

The frequency response was calculated for all wavelengths present in the FFT of the waveform, with the aim of performing the deconvolution of the waveforms. We have not performed the angular response analysis (unlike in [31]), since according to prediction in Fig. 2, the configuration with the fiber axis in line with the breakdown (0° tilt angle) offers the fastest response and was selected for all measurements.

III. Experimental Setup and Results

As pointed out above, a small interval Δt is required to achieve quick sensor response, also resulting in less signal distortion. Both the fast response together with a good signal-to-noise ratio of our measurement system are demonstrated in two cases: a pressure pulse emitted during the laser-induced breakdown generating a millimeter-sized bubble and a ten times smaller one.

LIB is first produced by an up to 15 mJ Nd:YAG laser pulse with a wavelength of 1064 nm and duration of 4 ns, focused by a lens system with a numerical aperture (NA) of 0.2 in water. In the second experiment, a different laser was used, delivering 70 ps, 10 μJ pulses, resulting in smaller size LIB plasma and approximately 150 μm-sized bubbles. In the second case, the final focusing is performed by a parabolic mirror inside a water container at NA 0.5, instead of the focusing lens depicted in Fig. 4.

Single-mode fiber (with diameters of core and cladding 5 and 125 μm, respectively, and mode field diameter of 6.6 μm) was used as the sensing element for pressure measurement. FOPH is positioned either in line with the incident laser light ("parallel" in Fig. 4), or perpendicular to it. In both cases, FOPH is oriented with no tilt ($\Phi \approx 0°$). The FOPH is mounted on a 3-D positioning stage enabling accurate positioning, however, slight misalignment of either position or orientation may be present, both characterized by tilt Φ as shown in Fig. 1. The reflected light in FOPH is detected by a 5 GHz photodiode (Thorlabs DET08CFC, operated on battery).

In the computer-controlled experimental setup, the transient voltage from the FOPH is recorded with an oscilloscope at 12 GHz analog bandwidth. A photodiode triggers both the oscilloscope and the illumination system, while the camera shutter is opened before the laser pulse and remains open for a few milliseconds. Additional details of the imaging setup are presented in [34].

First, a measurement close to breakdown induced by the 4 ns laser pulse, resulting in millimeter-sized bubbles is presented. FOPH is oriented perpendicular to the laser pulse axis direction and the generated plasma, resulting in a sharper shockwave than in the case of parallel orientation.

The shape of the oscilloscope signal (Fig. 5) demonstrates the need for extremely fast measurements to accurately record the pressure wave. The signal fall time in this case is 540 ps from 80% to 20%, with approximately 60 ns overall duration of the pressure disturbance (signal below initial value before the first recovery of the signal). The jagged pressure recovery indicates that the sensor also records the pressure transients from different parts of the breakdown arriving at (and departing from) the sensor at different times—note that the reflected shockwave from the fiber end did not yet have time to reach the fiber core for the first few oscillations, as the propagation takes approximately 40 ns. The noise of the signal can be lowered by digital filtering; Savitzky–Golay filter was used with order 2 and frame length corresponding to 250 ps before and after the point of interest. A sizeable reduction in noise was observed without the degradation of features such as signal fall time.

In Fig. 6(a), the pressure calculated using (2) and the deconvolution by the sensor frequency response function are

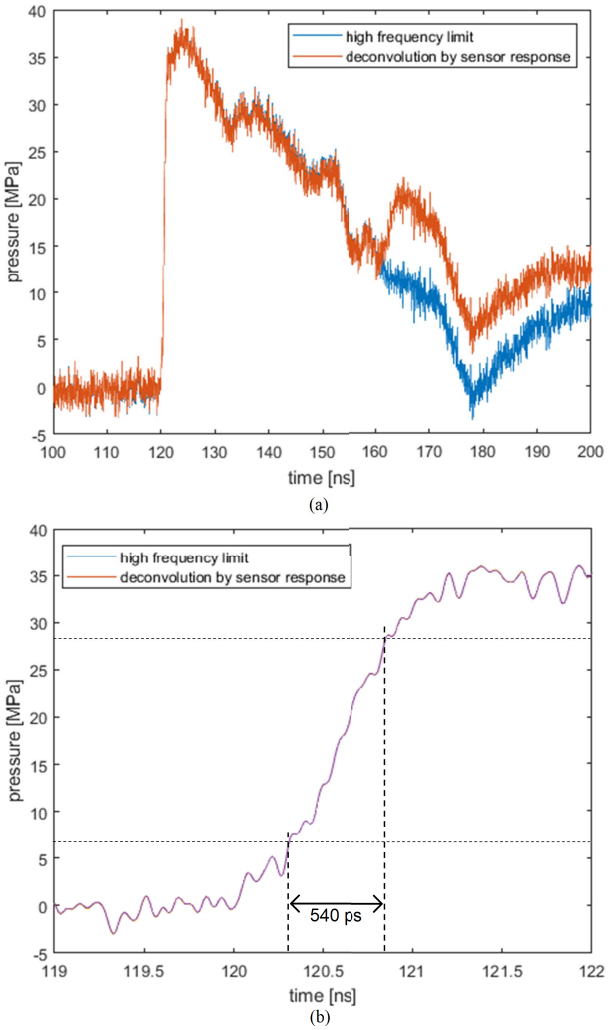

Fig. 6. (a) Orange: pressure calculated from voltage using the deconvolution by the sensor frequency response function shown in Fig. 3 and blue: pressure calculated from voltage, using the high-frequency limit of the response function, namely the constant of 2. In both cases, the peak pressure is the same. In (b) signal around 120 ns is zoomed in to emphasize the fast rise time from 20% to 80% of pressure in 540 ps.

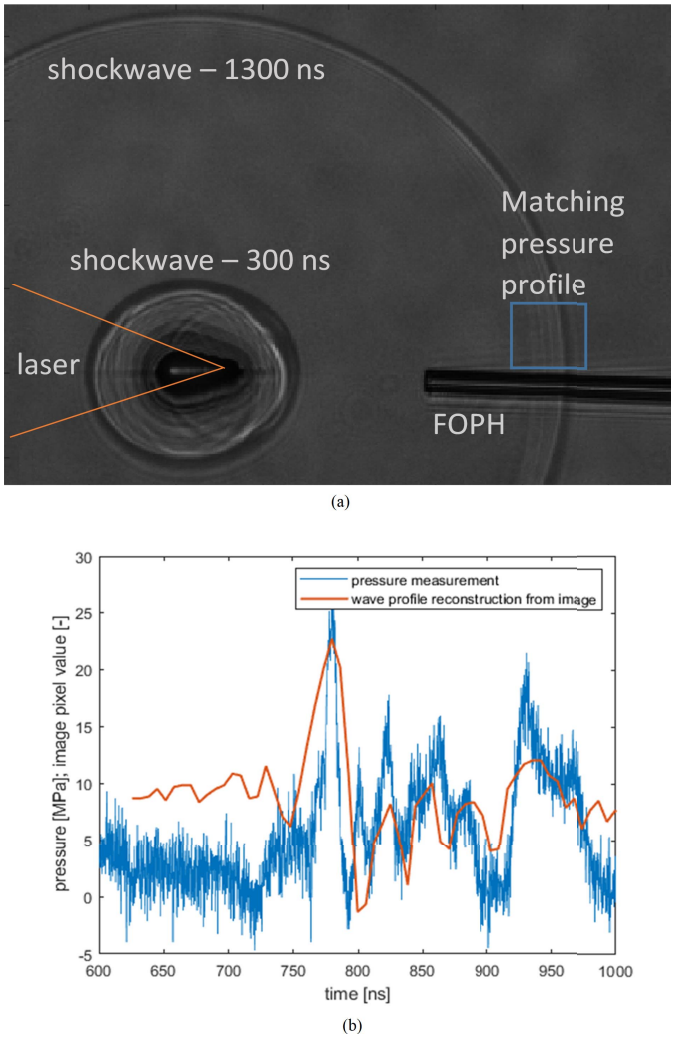

Fig. 7. Double-exposure image (a) taken simultaneously with FOPH trace (b) laser beam is parallel to the FOPH. Note that there is a single shockwave propagating away from the breakdown but is illuminated twice inside the frame, at 300 and 1300 ns. The voltage is converted to pressure using (2) and by applying deconvolution.

shown (orange) together with the calculated pressure using the high-frequency limit of the frequency response function, namely the constant value of 2 (blue). The two lines are indistinguishable at the peak where the pressure is measured to be 36 MPa. Most of the jagged responses in the signal appear to be real features of the shockwave which follows from the comparative analysis explained in Fig. 7. Zoom-in to shockwave rise time [Fig. 6(b)] shows the 540 ps shockwave rise time (from 20% to 80% of the signal). This pressure measurement is significantly faster than other reported shockwave measurements, for example in [36], [38], and is to the best of our knowledge the fastest measurement using FOPH. Both, the pressure calculated in the high-frequency limit (division by 2) and the deconvolved pressure practically match at this time scale, validating the high-frequency approximation for this shockwave analysis.

To validate the presented FOPH results, an image was taken simultaneously with the FOPH measurement—corresponding to the same breakdown.

Camera image [Fig. 7(a)] was taken with the shutter open before breakdown and with 2 illumination pulses at 300 and 1300 ns after the breakdown. Due to the finite size and the observed nonuniformity of the plasma, the emitted shockwave is apparently a sum of contributions from different locations inside the plasma. At a larger distance, the second illumination pulse reveals an evolved jagged shockwave in the direction parallel to the incident laser light, whereas a single sharp shockwave is observed in the direction perpendicular to the laser light. Pixel values were extracted from the image in a line in the matching pressure profile region marked in the image. Five parallel lines were averaged to improve the signal-to-noise ratio. The distance between the edges of shockwave for the 300 and 1300 ns illuminations was used to convert pixels to nanoseconds, one pixel corresponding to 6.5 ns. Pixel values were inverted (black corresponds to high pressure). The positions of the primary peaks of the image-based method and the FOPH measurement were aligned, and the other peaks show very good agreement between the image-based

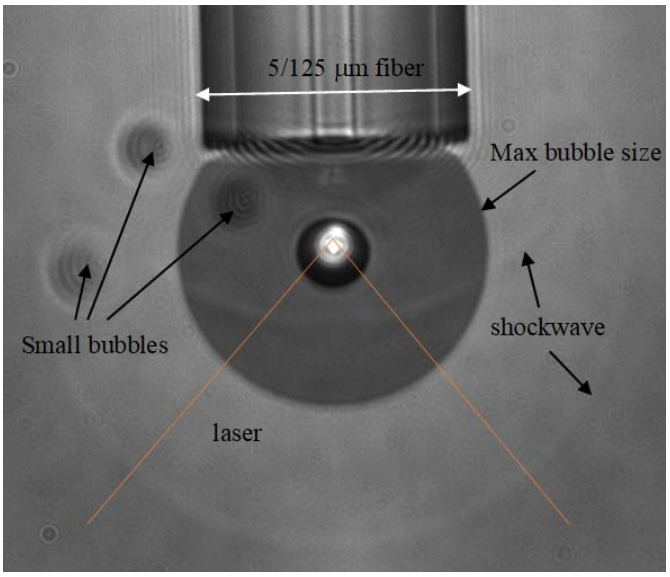

Fig. 8. Breakdown at approximately 40 μm distance from the fiber tip. Shockwave directly emitted from the breakdown as well as the part reflected from the fiber is visible. The second illumination pulse shows the bubble at maximum radius as well as three smaller bubbles.

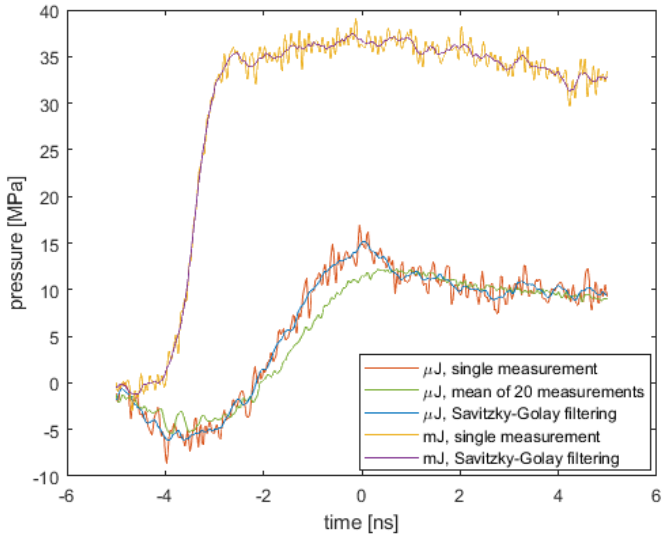

Fig. 9. FOPH measurement of shockwave pressure waveform generated by lower pulse energy, in comparison to higher pulse energy. Breakdown is at a distance of approximately 40 μm (breakdown to fiber); bubble at maximum radius (150 μm) engulfs fiber. The pressure is measured in the parallel direction as shown in Fig. 7. Scale at the bottom shows time from maximum pressure for both breakdowns.

shockwave measurement and the FOPH measurement [Fig. 7(b)], both in position and their relative amplitude.

FOPH pressure measurement was deconvolved by the calculated sensor response to obtain true measured pressure, which is 26 MPa at maximum. This is lower than in the direction perpendicular to breakdown (36 MPa), in agreement with [39]. However, we improve on their measurements by also showing that the pressure rise time differs—5 ns pressure rise time was observed in the direction parallel to the incident laser [Fig. 7(b)], whereas only 540 ps rise time was observed in the direction perpendicular to the incident laser light [Fig. 6(b)].

Beyond the validation of approaches, the image [Fig. 7(a)] shows the 2-D profile of the pressure front as well as the wavefront evolution with distance (due to multiple illuminations). These shockwave characteristics are impossible to be extracted from a single hydrophone measurement. On the other hand, FOPH measures both more locally (each pixel corresponds to approximately 10 μm whereas fiber core has 5 μm diameter) and with significantly better time resolution (each pixel in the image corresponds to 6.5 ns whereas the oscilloscope and the photodiode have better than 0.2 ns resolution). The improved time resolution is also the key behind the observation of the jagged shockwave in the direction perpendicular to the incident laser [Fig. 6(a)]—the image-based method had an insufficient temporal resolution to distinguish these small variations. Owing to the presented comparative analysis of the parallel case, we are confident to believe that also in the perpendicular case the recorded waveform shows accurate pressure time dependence. Therefore, the two methods complement each other.

Furthermore, the image is valuable to guide the fiber positioning, which is especially important for the close measurement of pressure waves from small bubbles. For these bubbles, the deposited energy is significantly lower, resulting in a much weaker pressure wave. To achieve a sufficient signal-to-noise ratio, the fiber needs to be positioned very close to the breakdown; however, accidental positioning of the fiber directly at the breakdown site is likely to cause damage to the fiber tip.

The image taken of the very small breakdown (Fig. 8) shows the breakdown (white), accompanied by a darker circle, which is the bubble size at the first illumination pulse. The shockwave in the lower and the middle part of the picture is also visible due to the first illumination pulse. The reflection of the shockwave from the fiber seems to have the same intensity as the direct wave, suggesting that most of the shockwave energy arriving at the fiber is reflected. Fiber diameter (125 μm) is used as a scale bar, while the fiber core appears larger due to lensing through the fiber cladding.

The second illumination pulse shows the bubble at maximum size (diameter of approximately 150 μm). Because the separation is small, the bubble at maximum radius touches the fiber and is slightly deformed. The second illumination pulse also shows three smaller bubbles. Such small bubbles are often present, but do not interfere with the measurements unless they are located at the fiber end face at the time of the measurement.

Pressure measurement of a shockwave accompanying lower energy LIB is shown in Fig. 9.

The bubble is smaller (150 μm diameter) and the pressure pulse significantly lower and shorter than in the case of the millimeter-sized bubble, despite a much smaller distance between the breakdown site and the sensor. The peak pressure of 15 MPa is measured at a very short distance of 40 μm from breakdown. The initial pressure rise time is approximately 1.5 ns while the full duration of the shockwave (not shown here) is below 20 ns—short enough so that the edge wave from the fiber end does not yet propagate to the sensing area

to contribute to the signal. Given the very small distance between the breakdown and the sensor, the multimode fiber sensor would be incapable to accurately measure such a short rise time (Fig. 2). The repeatabilities of both the breakdown and the FOPH measurement are shown by good agreement of the single measurement and the average of 20 measurements, showing that the signal-to-noise ratio may be improved by averaging, as well as good repeatability of the breakdown. As an alternative to multiple measurements, digital filtering of data is an option. Savitzky–Golay filtering with polynomial order of 2 and a window of 250 ps before and after the point of interest is shown. The filtered signal retains all shockwave features and does not change the pressure rise time while it effectively suppresses the noise. Filtering is especially helpful to automatically extract shockwave pressure rise time, which would be otherwise difficult for the lower pressure shockwaves generated during microjoule energy breakdown which has a lower signal-to-noise ratio.

The approximately 20 ns shockwave duration (not shown) is smaller compared to shockwaves generated with millijoule energy laser pulses which have nanosecond shockwave duration [Fig. 6(a)].

Shockwave generated during nanosecond pulse breakdown exhibits significantly longer shockwave duration, as well as slightly shorter pressure rise time. However, there are several significant differences between the measured pressures, making a direct comparison between these two experiments difficult. Namely, there are differences in: 1) the source energy, 2) the distance from the detector and the plasma, and 3) the shape of the plasma. Systematic experiments are required to characterize the shockwaves in the close proximity of the source—plasma in our presented experiments. We believe that with the new very local and very fast single-mode FOPH sensor, supported by simultaneous multiple exposure imaging, the results will bring new insights on the shockwave generation and evolution close to the source.

IV. Conclusion

Using our custom single-mode FOPH, the pressure waveform of a shockwave arising from LIB was measured. Due to the fast and localized sensor response that is enabled by the single-mode fiber small sensing area, we are able to measure pressure transients with significantly better resolution (spatial and temporal) than with FOPH employing multimode fiber. This is demonstrated by the measurement of the pressure rise time well below 1 ns, which is to our knowledge the first such measurement using fiber-optic hydrophones, as well as by accurate measurement of shockwave pressure profile, as indicated by qualitative validation using additional analysis of the complementary image-based method, where the recorded shock waveform was shown to follow the pressure distribution as deduced from the image.

The imaging method also enabled accurate sensor positioning to measure shockwaves arising from a LIB generated with a 10 μJ laser pulse at a distance between the breakdown and the FOPH as small as 40 μm where a high pressure of 15 MPa was measured despite low laser pulse energy in the millijoules range. The recorded rise time of 1.5 ns is shorter than could be measured using multimode fiber-based FOPH at the same distance.

The presented novel sensor configuration will be very useful in studying the shockwaves in contemporary medical and industrial applications employing pulsed laser effects in aqueous materials.

References

[1] M. Dell'Aglio, R. Alrifai, and A. De Giacomo, "Nanoparticle enhanced laser induced breakdown spectroscopy (NELIBS), a first review," *Spectrochim. Acta B, At. Spectrosc.*, vol. 148, pp. 105–112, Oct. 2018, doi: 10.1016/j.sab.2018.06.008.

[2] H. Lim, D. Jang, D. Kim, J. W. Lee, and J.-M. Lee, "Correlation between particle removal and shock-wave dynamics in the laser shock cleaning process," *J. Appl. Phys.*, vol. 97, no. 5, Mar. 2005, Art. no. 054903, doi: 10.1063/1.1857056.

[3] C. D. Ohl *et al.*, "Sonoporation from jetting cavitation bubbles," *Biophys. J.*, vol. 91, pp. 4285–4295, Dec. 2006, doi: 10.1529/biophysj.105.075366.

[4] Y. Kang *et al.*, "Tumor vasodilation by N-heterocyclic carbene-based nitric oxide delivery triggered by high-intensity focused ultrasound and enhanced drug homing to tumor sites for anti-cancer therapy," *Biomaterials*, vol. 217, Oct. 2019, Art. no. 119297, doi: 10.1016/j.biomaterials.2019.119297.

[5] T. Kroczak, K. B. Scotland, B. Chew, and K. T. Pace, "Shockwave lithotripsy: Techniques for improving outcomes," *World J. Urol.*, vol. 35, no. 9, pp. 1341–1346, Sep. 2017, doi: 10.1007/s00345-017-2056-y.

[6] K. B. Bader, E. Vlaisavljevich, and A. D. Maxwell, "For whom the bubble grows: Physical principles of bubble nucleation and dynamics in histotripsy ultrasound therapy," *Ultrasound Med. Biol.*, vol. 45, no. 5, pp. 1056–1080, May 2019, doi: 10.1016/j.ultrasmedbio.2018.10.035.

[7] V. A. Shaimova *et al.*, "Evaluation of YAG-laser vitreolysis effectiveness based on quantitative characterization of vitreous floaters," *Vestnik Oftal'mologii*, vol. 134, no. 1, p. 56, 2018, doi: 10.17116/oftalma2018134156-62.

[8] A. Vogel, S. Busch, and U. Parlitz, "Shock wave emission and cavitation bubble generation by picosecond and nanosecond optical breakdown in water," *J. Acoust. Soc. Amer.*, vol. 100, no. 1, pp. 148–165, Jul. 1996.

[9] Y. Li, Z. Yang, G. Wang, and C. Yang, "Research on piezoelectric pressure sensor for shock wave load measurement," *ISA Trans.*, vol. 104, pp. 382–392, Sep. 2020, doi: 10.1016/j.isatra.2020.05.018.

[10] P. A. Lewin, "Miniature piezoelectric polymer ultrasonic hydrophone probes," *Ultrasonics*, vol. 19, no. 5, pp. 213–216, Sep. 1981, doi: 10.1016/0041-624X(81)90005-6.

[11] K. A. Wear, C. Baker, and P. Miloro, "Directivity and frequency-dependent effective sensitive element size of membrane hydrophones: Theory versus experiment," *IEEE Trans. Ultrason., Ferroelectr., Freq. Control*, vol. 66, no. 11, pp. 1723–1730, Nov. 2019, doi: 10.1109/TUFFC.2019.2930042.

[12] O. V. Bessonova and V. Wilkens, "Membrane hydrophone measurement and numerical simulation of HIFU fields up to developed shock regimes," *IEEE Trans. Ultrason., Ferroelectr., Freq. Control*, vol. 60, no. 2, pp. 290–300, Feb. 2013, doi: 10.1109/TUFFC.2013.2565.

[13] V. Wilkens and W. Molkenstruck, "Broadband PVDF membrane hydrophone for comparisons of hydrophone calibration methods up to 140 MHz," *IEEE Trans. Ultrason., Ferroelectr., Freq. Control*, vol. 54, no. 9, pp. 1784–1791, Sep. 2007, doi: 10.1109/TUFFC.2007.462.

[14] IEEE. (2018). *13th IEEE International Conference on Industry Applications (INDUSCON)*. Accessed: Oct. 29, 2020. [Online]. Available: https://ieeexplore.ieee.org/servlet/opac?punumber=8609865

[15] B. Fay, G. Ludwig, C. Lankjaer, and P. A. Lewin, "Frequency response of PVDF needle-type hydrophones," *Ultrasound Med. Biol.*, vol. 20, no. 4, pp. 361–366, 1994, doi: 10.1016/0301-5629(94)90004-3.

[16] J. Staudenraus and W. Eisenmenger, "Fibre-optic probe hydrophone for ultrasonic and shock-wave measurements in water," *Ultrasonics*, vol. 31, no. 2, pp. 267–273, 1993.

[17] P. A. Anderson *et al.*, "Characterizing shock waves in hydrogel using high speed imaging and a fiber-optic probe hydrophone," *Phys. Fluids*, vol. 29, no. 5, May 2017, Art. no. 057101, doi: 10.1063/1.4982062.

[18] P. C. Beard, A. M. Hurrell, and T. N. Mills, "Characterization of a polymer film optical fiber hydrophone for use in the range 1 to 20 MHz: A comparison with PVDF needle and membrane hydrophones," *IEEE Trans. Ultrason., Ferroelectr., Freq. Control*, vol. 47, no. 1, pp. 256–264, Jan. 2000, doi: 10.1109/58.818769.

[19] J. Haller *et al.*, "A comparative evaluation of three hydrophones and a numerical model in high intensity focused ultrasound fields," *J. Acoust. Soc. Amer.*, vol. 131, no. 2, pp. 1121–1130, 2012.
[20] Z. Meng, W. Chen, J. Wang, X. Hu, M. Chen, and Y. Zhang, "Recent progress in fiber-optic hydrophones," *Photon. Sensors*, vol. 11, no. 1, pp. 109–122, Mar. 2021, doi: 10.1007/s13320-021-0618-5.
[21] P. Morris, A. Hurrell, A. Shaw, E. Zhang, and P. Beard, "A Fabry–Pérot fiber-optic ultrasonic hydrophone for the simultaneous measurement of temperature and acoustic pressure," *J. Acoust. Soc. Amer.*, vol. 125, no. 6, pp. 3611–3622, Jun. 2009, doi: 10.1121/1.3117437.
[22] S. Pevec and D. Donlagic, "Multiparameter fiber-optic sensor for simultaneous measurement of thermal conductivity, pressure, refractive index, and temperature," *IEEE Photon. J.*, vol. 9, no. 1, pp. 1–14, Feb. 2017, doi: 10.1109/JPHOT.2017.2651978.
[23] P. C. Beard and T. N. Mills, "Extrinsic optical-fiber ultrasound sensor using a thin polymer film as a low-finesse Fabry–Pérot interferometer," *Appl. Opt.*, vol. 35, no. 4, pp. 663–675, 1996, doi: 10.1364/AO.35.000663.
[24] Z. Shao, Q. Rong, F. Chen, and X. Qiao, "High-spatial-resolution ultrasonic sensor using a micro suspended-core fiber," *Opt. Exp.*, vol. 26, no. 8, p. 10820, Apr. 2018, doi: 10.1364/OE.26.010820.
[25] H. Chen, Z. Shao, Y. Hao, and Q. Rong, "A high-frequency hydrophone using an optical fiber microknot resonator," *Opt. Commun.*, vol. 446, pp. 77–83, Sep. 2019, doi: 10.1016/j.optcom.2019.04.071.
[26] C. Koch and K.-V. Jenderka, "Measurement of sound field in cavitating media by an optical fibre-tip hydrophone," *Ultrason. Sonochem.*, vol. 15, no. 4, pp. 502–509, Apr. 2008, doi: 10.1016/j.ultsonch.2007.05.007.
[27] H. Xinjing *et al.*, "Low-cost, high-sensitivity hydrophone based on resonant air cavity," *IEEE Sensors J.*, vol. 21, no. 6, pp. 7348–7357, Mar. 2021, doi: 10.1109/JSEN.2020.3048066.
[28] A. Hurrell and P. Beard, "Piezoelectric and fibre-optic hydrophones," in *Ultrasonic Transducers*. Amsterdam, The Netherlands: Elsevier, 2012, pp. 619–676.
[29] A. Arvengas, K. Davitt, and F. Caupin, "Fiber optic probe hydrophone for the study of acoustic cavitation in water," *Rev. Sci. Instrum.*, vol. 82, no. 3, Mar. 2011, 034904, doi: 10.1063/1.3557420.
[30] B. Shen, Y. Wada, D. Koyama, R. Isago, Y. Mizuno, and K. Nakamura, "Fiber-optic ultrasonic probe based on refractive-index modulation in water," *Proc. SPIE*, vol. 7753, May 2011, Art. no. 77539W, doi: 10.1117/12.884961.
[31] J. F. Krucker, A. Eisenberg, M. Krix, R. Lötsch, M. Pessel, and H. G. Trier, "Rigid piston approximation for computing the transfer function and angular response of a fiber-optic hydrophone," *J. Acoust. Soc. Amer.*, vol. 107, no. 4, pp. 1994–2003, Apr. 2000, doi: 10.1121/1.428483.
[32] K. A. Wear, A. Shah, and C. Baker, "Correction for hydrophone spatial averaging artifacts for circular sources," *IEEE Trans. Ultrason., Ferroelectr., Freq. Control*, vol. 67, no. 12, pp. 2674–2691, Dec. 2020, doi: 10.1109/TUFFC.2020.3007808.
[33] L. Shi *et al.*, "A fiber optoacoustic emitter with controlled ultrasound frequency for cell membrane sonoporation at submillimeter spatial resolution," *Photoacoustics*, vol. 20, Dec. 2020, Art. no. 100208, doi: 10.1016/j.pacs.2020.100208.
[34] V. Agrež and T. Požar, "High-speed photography of shock waves with an adaptive illumination," *Opt. Lett.*, vol. 45, no. 6, p. 1547, Mar. 2020, doi: 10.1364/OL.388444.
[35] P. Schiebener, J. Straub, J. M. H. L. Sengers, and J. S. Gallagher, "Refractive index of water and steam as function of wavelength, temperature and density," *J. Phys. Chem. Reference Data*, vol. 19, no. 3, pp. 677–717, Feb. 1990.
[36] G. Berkovic *et al.*, "Ultrafast pressure measurement in shock wave research using fiber Bragg grating sensors," *Proc. SPIE*, vol. 10654, May 2018, Art. no. 106540S, doi: 10.1117/12.2302801.
[37] A. G. Doukas, A. D. Zweig, J. K. Frisoli, R. Birngruber, and T. F. Deutsch, "Non-invasive determination of shock wave pressure generated by optical breakdown," *Appl. Phys. B, Lasers Opt.*, vol. 53, no. 4, pp. 237–245, Oct. 1991.
[38] G. Sinibaldi *et al.*, "Laser induced cavitation: Plasma generation and breakdown shockwave," *Phys. Fluids*, vol. 31, no. 10, Oct. 2019, Art. no. 103302, doi: 10.1063/1.5119794.
[39] Y. Tagawa, S. Yamamoto, K. Hayasaka, and M. Kameda, "On pressure impulse of a laser-induced underwater shock wave," *J. Fluid Mech.*, vol. 808, pp. 5–18, Dec. 2016, doi: 10.1017/jfm.2016.644.

Jaka Petelin was born in Ljubljana, Slovenia, in 1985. He received the B.S. and Ph.D. degrees from the University of Ljubljana, Ljubljana, Slovenia, in 2010 and 2015, respectively.

From 2010 to 2016, he worked as a Senior Researcher with LPKF Laser & Electronics d.o.o., Garbsen, Germany. In 2016, he joined the Faculty of Mechanical Engineering, University of Ljubljana, where he is working with the Laboratory for Photonics and Laser Systems. His research interest includes the development of new laser sources and their application for industry and medicine.

Žiga Lokar received the B.Sc. and Ph.D. degrees from the University of Ljubljana, Ljubljana, Slovenia, in 2011 and 2019, respectively.

In 2018, he joined the Laboratory for Photonics and Laser Systems with the Faculty of Mechanical Engineering, University of Ljubljana. His current research interest includes the study of light-induced breakdown in water and other liquids, together with associated phenomena (shockwave, bubble, jetting).

Darja Horvat received the B.Sc. and M.Sc. degrees in physics from the Faculty of Mathematics and Physics, University of Ljubljana, Ljubljana, Slovenia, in 1989 and 2000, respectively, where she received the Ph.D. degree from the Faculty of Mechanical Engineering, in 2004.

She is with the Faculty of Mechanical Engineering, University of Ljubljana. Her research interests include laser ultrasonics and the interaction of laser light with matter, mostly fluids.

Rok Petkovšek was born in Ljubljana, Slovenia, in 1969. He received the B.S. and M.S. degrees in physics and the Ph.D. degree from the University of Ljubljana, Ljubljana, Slovenia in 1994, 1999, and 2003, respectively.

From 1995 to 2003, he worked as a Researcher with Jozef Stefan Institute, Ljubljana. In 2003, he joined the Faculty of Mechanical Engineering, University of Ljubljana, as a Senior Researcher. There he founded a new Laboratory for Photonics and Laser Systems in 2016. He has served as the Head ever since. Since 2016, he has been the Chair of the Department of Optodynamics and Laser Technology, Faculty of Mechanical Engineering, University of Ljubljana. He has published more than 50 peer-reviewed journal articles. His research interest includes the development of new laser sources and their application for industry and medicine.